Journal of Systems Engineering and Electronics
Vol. PP, No. 99, November 2023, pp.1 – 10

Improved spatio-temporal alignment measurement method for hull deformation

XU Dongsheng[1,2], YU Yuanjin[1,*], ZHANG Xiaoli[2], and PENG Xiafu[2]

1. School of Automation, Beijing Institute of Technology, Beijing 100081, China;
2. School of Aerospace Engineering, Xiamen University, Xiamen 361005, China

Abstract: In this paper, an improved spatio-temporal alignment measurement method is presented to address the inertial matching measurement of hull deformation under the coexistence of time delay and large misalignment angle. Large misalignment angle and time delay often occur simultaneously and bring great challenges to the accurate measurement of hull deformation in space and time. The proposed method utilizes coarse alignment with large misalignment angle and time delay estimation of inertial measurement unit modeling to establish a brand-new spatio-temporal aligned hull deformation measurement model. In addition, two-step loop control is designed to ensure the accurate description of dynamic deformation angle and static deformation angle by the time-space alignment method of hull deformation. The experiments illustrate that the proposed method can effectively measure the hull deformation angle when time delay and large misalignment angle coexist.

Keywords: inertial measurement, spatio-temporal alignment, hull deformation.

DOI: 10.23919/JSEE.2023.000139

1. Introduction

With the rapid development of marine technology, modern warships are usually equipped with radar systems, shipborne missiles, and other shipborne equipment. Therefore, it is necessary to establish a unified space reference for the whole ship to ensure the performance of shipborne equipment [1-3]. In fact, the hull is not a rigid body. During sailing, the hull is subject to flexure deformation. Therefore, the real-time measurement of hull deformation is of great significance to the establishment of a unified spatial reference for the whole ship [4]. Benefiting from the advantages of independence, continuous measurement and low installation cost, inertial measurement method has become one of the most promising hull deformation measurement methods in recent years [5,6].

The hull deformation angle consists of static deformation angle and dynamic deformation angle [7,8]. The static deformation angle is mainly caused by the long-term influence of structural aging, thermal expansion and cold contraction caused by sunshine and other factors. Generally, the static deformation angle is not an absolutely constant during a long voyage, but changes very slowly with time. Zheng et al. simplified the long-term quasi-static deformation angle model into a random walk process [9]. The dynamic deformation angle is usually a short-period angular deformation caused by external forces such as wave impact, hull emergency steering, and so on. It is commonly modeled as a second-order Markov model driven by white noise [10,11].

Inertial measurement system often installs one set of inertial measurement unit (IMU) nearby the main navigation system, and also install another set of IMU nearby the user equipment. Inertial matching method measures hull deformation angle by utilizing output differences between the IMUs [7,12,13]. The difference is used as an observed measurement to establish the measurement model of hull deformation inertial matching method [14]. Then, the model with noise is substituted into Kalman filter to accurately calculate the hull deformation angle [15-17]. The interacting multiple model Kalman filtering in [18] was utilized to improve the accuracy of filtering operation of hull deformation with uncertain model parameters. Neural extended Kalman filter proposed by Kramer et al. was used to adaptively match the model error [19].

In the inertial measurement of hull deformation, the large misalignment angle can introduce nonlinear error in space into the inertial measurement model, which no longer meets the small angle assumption of traditional inertial matching measurement and causes the decrease of measurement result accuracy. He et al. derived inertial matching method based on attitude quaternion for hull deformation measurement with large azimuth misalignment angle [20]. At the same time, if there is an informa-

Manuscript received June 27, 2022.
*Corresponding author.
This work was supported in part by the Beijing Insititute of Technology Research Fund program for Young Scholars (2020X04104)

tion acquisition delay between the two sets of inertial measurement unit, time delay will bring nonlinear errors to the inertial measurement model of hull deformation and decrease the convergence precision of measurement results. Wang et al. proposed an adaptive variable parameter multiple model to compensate the time delay when the measurement noise parameters and model parameters are uncertain [21]. However, the large misalignment angle and sampling time delay often appear in the inertial matching measurement of hull deformation at the same time. There are few methods to solve these problems at the same time in previous research work. Therefore, the problem of time and space synchronous alignment inertial matching measurement of hull deformation needs to be solved urgently.

In order to solve these problems, an inertial measurement method for spatio-temporal alignment of hull deformation is proposed in this paper. A brand-new hull deformation inertial matching model is deduced to compensate for the nonlinear error caused by large misalignment angle and time delay. The proposed method makes full use of coarse alignment of quaternion optimization and IMU output modeling, and derives a brand-new hull deformation model with the condition of large misalignment angle and time delay. The neural network Kalman filter (NNKF) is utilized to complete the state estimation for its nonlinear tolerance, and the two steps feedback loop is designed to ensure the coarse alignment of large misalignment angle under the time delay.

The remainder of this paper unfolds as follows: Section 2 briefly introduces the proposed spatio-temporal alignment model for hull deformation. In Section 3, the hull deformation system state equation is established, and the loop design based on Kalman filter is introduced. Section 4 carries out the experiments to verify the effectiveness of the proposed method. Section 5 draws the conclusions.

2. Spatio-temporal alignment model for hull deformation

The hull deformation inertial matching measurement system installs two sets of IMU, which are respectively installed near the main navigation system and user device side, as shown in Fig. 1.

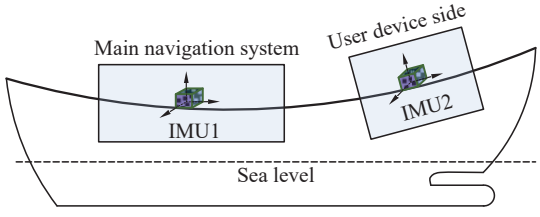

Fig. 1 IMU installation

The coordinate systems definition involved in inertial matching method of hull deformation are denoted as follows:

i_1, i_2: Ideal inertial coordinate system of IMU1, IMU2.

$\tilde{i}_1$, $\tilde{i}_2$: Calculation inertial coordinate system drifting from i_1, i_2, which is caused by gyro drift in IMU1 and IMU2.

b_1, b_2: Carrier coordinate system of IMU1, IMU2.

According to the coordinate definition, the attitude matrix output of IMU2 can be expressed as

$$\boldsymbol{C}_{b_2}^{\tilde{i}_2} = \boldsymbol{C}_{i_2}^{\tilde{i}_2}\boldsymbol{C}_{i_1}^{i_2}\boldsymbol{C}_{\tilde{i}_1}^{i_1}\boldsymbol{C}_{b_1}^{\tilde{i}_1}\boldsymbol{C}_{b_2}^{b_1}. \tag{1}$$

If real time hull deformation angle $\boldsymbol{\varphi}$ satisfy the assumption of small angle, $\boldsymbol{C}_{b_2}^{b_1}$ [7] can be expressed as

$$\boldsymbol{C}_{b_2}^{b_1} \approx \boldsymbol{I} + \begin{bmatrix} 0 & -\varphi_z & \varphi_y \\ \varphi_z & 0 & -\varphi_x \\ -\varphi_y & \varphi_x & 0 \end{bmatrix} = \boldsymbol{I} + [\boldsymbol{\varphi}\times]. \tag{2}$$

However, under the condition of large misalignment angle, $\boldsymbol{C}_{b_2}^{b_1}$ and $\boldsymbol{\varphi}$ no longer meet the relationship of (2) because large angle bring great nonlinear error to the model. To solve the large misalignment angle problem, the hull deformation angle $\boldsymbol{\varphi}$ is divided into two parts to calculate, including the large angle $\boldsymbol{\varphi}_{02}$ obtained by coarse alignment and the residual small angle $\boldsymbol{\varphi}_{10}$. As shown in Fig. 2, b_0 and i_0 are obtained by the coarse alignment as a virtual coordinate system rotating from b_2 and i_2, respectively. Attitude transfer matrix $\boldsymbol{C}_{b_2}^{b_1}$, $\boldsymbol{C}_{b_0}^{b_1}$, and $\boldsymbol{C}_{b_2}^{b_0}$ corresponds to Euler angle $\boldsymbol{\varphi}$, $\boldsymbol{\varphi}_{10}$, and $\boldsymbol{\varphi}_{02}$, respectively.

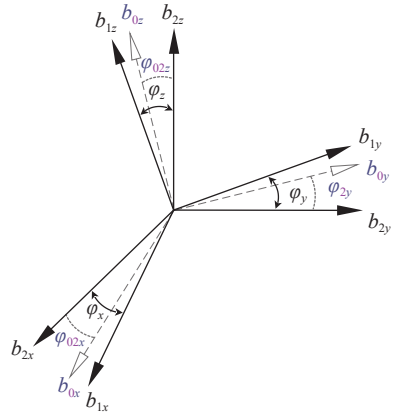

Fig. 2 Coordinate definition for spatio-temporal alignment in the hull deformation measurement

$$\boldsymbol{\varphi} = \boldsymbol{\varphi}_{10} + \boldsymbol{\varphi}_{02} \tag{3}$$

$$\boldsymbol{C}_{b_2}^{b_1} = \boldsymbol{C}_{b_0}^{b_1}\boldsymbol{C}_{b_2}^{b_0} \tag{4}$$

$\boldsymbol{C}_{b_2}^{b_0}$ in (4) chooses quaternion optimization method proposed by Lu et al. in [22] to complete the coarse alignment because of its great robustness and accuracy in

coarse estimation of misalignment angle. Let $\boldsymbol{\alpha}(t)$ and $\boldsymbol{\beta}(t)$ be the angular velocity output integral from time 0 to time t of IMU2 and IMU1, respectively. The $\boldsymbol{C}_{b_2}^{b_0}$ can be expressed as

$$\boldsymbol{\beta}(t) \approx \boldsymbol{C}_{b_2}^{b_0}\boldsymbol{\alpha}(t). \tag{5}$$

After denoting the quaternion of $\boldsymbol{C}_{b_2}^{b_0}$ as $\boldsymbol{q} = [s, \eta]^{\mathrm{T}}$, (5) can be written as

$$\boldsymbol{\beta}(t) = \boldsymbol{q} \otimes \boldsymbol{\alpha}(t) \otimes \boldsymbol{q}^{*} \tag{6}$$

where $\otimes$ is the quaternion multiplication operator, and * is the quaternion conjugate operator.

By defining operators

$$\begin{bmatrix} + \\ \boldsymbol{q} \end{bmatrix} = \begin{bmatrix} s & -\boldsymbol{\eta}^{\mathrm{T}} \\ \boldsymbol{\eta} & s\boldsymbol{I} + \boldsymbol{\eta}(\times) \end{bmatrix}$$

and

$$\begin{bmatrix} - \\ \boldsymbol{q} \end{bmatrix} = \begin{bmatrix} s & -\boldsymbol{\eta}^{\mathrm{T}} \\ \boldsymbol{\eta} & s\boldsymbol{I} - \boldsymbol{\eta}(\times) \end{bmatrix},$$

(6) can be expressed as in a linear form as follows:

$$\left(\begin{bmatrix} + \\ \boldsymbol{\beta}(t) \end{bmatrix} - \begin{bmatrix} - \\ \boldsymbol{\alpha}(t) \end{bmatrix} \right) \boldsymbol{q} = 0. \tag{7}$$

Let

$$\boldsymbol{K} = \int_0^t \left(\begin{bmatrix} + \\ \boldsymbol{\beta}(t) \end{bmatrix} - \begin{bmatrix} - \\ \boldsymbol{\alpha}(t) \end{bmatrix} \right)^{\mathrm{T}} \left(\begin{bmatrix} + \\ \boldsymbol{\beta}(t) \end{bmatrix} - \begin{bmatrix} - \\ \boldsymbol{\alpha}(t) \end{bmatrix} \right) \mathrm{d}t,$$

and the minimum eigenvalue of matrix $\boldsymbol{K}$ can be obtained. The normalized eigenvector corresponding to the minimum eigenvalue is the optimal quaternion corresponding to attitude transfer matrix $\boldsymbol{C}_{b_2}^{b_0}$, so that the coarse alignment result $\boldsymbol{C}_{b_2}^{b_0}$ is obtained [22].

$\boldsymbol{C}_{b_0}^{b_1}$ can be expressed by $\boldsymbol{C}_{b_2}^{b_0}$ as follows by the coordinate definition:

$$\boldsymbol{C}_{b_0}^{b_1} = \boldsymbol{C}_{b_1}^{\tilde{i}_1\,\mathrm{T}} \boldsymbol{C}_{\tilde{i}_1}^{i_1\,\mathrm{T}} \boldsymbol{C}_{i_0}^{i_1} \boldsymbol{C}_{i_2}^{i_0} \boldsymbol{C}_{\tilde{i}_2}^{i_2} \boldsymbol{C}_{b_2}^{\tilde{i}_2} \boldsymbol{C}_{b_0}^{b_2}. \tag{8}$$

For the time delay problem in hull deformation measurement, time delay Δt between IMU1 and IMU2 is introduced into the improved method. As shown in Fig. 3, because of the time delay, the data of IMU2, which should have been acquired at t_n, is not received until $\tilde{t}_n$ after Δt passed. The real-time output attitude matrix of IMU2, i.e., $\boldsymbol{C}_{b_2}^{\tilde{i}_2}$, can be written by first order expansion of Taylor formula with the higher order terms $\boldsymbol{R}_n(t)$ at time t.

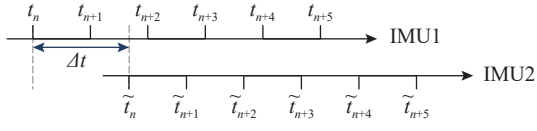

Fig. 3 Output time delay between IMU1 and IMU2

$$\boldsymbol{C}_{b_2}^{\tilde{i}_2}(t) = \boldsymbol{C}_{b_2}^{\tilde{i}_2}(t) + \dot{\boldsymbol{C}}_{b_2}^{\tilde{i}_2}(t)\ \Delta\boldsymbol{t} + \boldsymbol{R}_n(t) \tag{9}$$

Let $\boldsymbol{q} = [q_1, q_2, q_3, q_4]^{\mathrm{T}}$ be the attitude quaternion of $\boldsymbol{C}_{b_2}^{\tilde{i}_2}$, so the $\dot{\boldsymbol{C}}_{b_2}^{\tilde{i}_2}$ in (8) can be calculated as

$$\dot{\boldsymbol{C}}_{b_2}^{\tilde{i}_2} = \frac{\partial \boldsymbol{C}_{b_2}^{\tilde{i}_2}}{\partial q_1}\dot{q}_1 + \frac{\partial \boldsymbol{C}_{b_2}^{\tilde{i}_2}}{\partial q_2}\dot{q}_2 + \frac{\partial \boldsymbol{C}_{b_2}^{\tilde{i}_2}}{\partial q_3}\dot{q}_3 + \frac{\partial \boldsymbol{C}_{b_2}^{\tilde{i}_2}}{\partial q_4}\dot{q}_4. \tag{10}$$

From (9) and (10), by ignoring the higher order terms $R_n(t)$, we have

$$\boldsymbol{C}_{i_2}^{\tilde{i}_2} \boldsymbol{C}_{i_0}^{i_2} \boldsymbol{C}_{i_1}^{i_0} \boldsymbol{C}_{\tilde{i}_1}^{i_1} \boldsymbol{C}_{b_1}^{\tilde{i}_1} \boldsymbol{C}_{b_0}^{b_1} \boldsymbol{C}_{b_2}^{b_0} = \boldsymbol{C}_{b_2}^{\tilde{i}_2} + \dot{\boldsymbol{C}}_{b_2}^{\tilde{i}_2} \cdot \Delta\boldsymbol{t}. \tag{11}$$

The real time attitude transfer matrix between b_0 and b_1 is $\boldsymbol{C}_{b_0}^{b_1}$ with a small Euler angle $\boldsymbol{\varphi}_{10}$:

$$\boldsymbol{C}_{b_0}^{b_1} \approx \boldsymbol{I} + \begin{bmatrix} 0 & -\varphi_{10z} & \varphi_{10y} \\ \varphi_{10z} & 0 & -\varphi_{10x} \\ -\varphi_{10y} & \varphi_{10x} & 0 \end{bmatrix} = \boldsymbol{I} + [\boldsymbol{\varphi}_{10}\times]. \tag{12}$$

According to the coordinate definition, $\boldsymbol{C}_{i_1}^{i_0}$ represents the initial small angle at initial time t_0. Let $\boldsymbol{\varphi}_0$ be the Euler angle of the initial small angle:

$$\boldsymbol{C}_{i_1}^{i_0} \approx \boldsymbol{I} - \begin{bmatrix} 0 & -\varphi_{0z} & \varphi_{0y} \\ \varphi_{0z} & 0 & -\varphi_{0x} \\ -\varphi_{0y} & \varphi_{0x} & 0 \end{bmatrix} = \boldsymbol{I} - [\boldsymbol{\varphi}_0\times]. \tag{13}$$

The gyro drift Euler angle of IMU1 and IMU2 are denoted by $\boldsymbol{\theta}_1$ and $\boldsymbol{\theta}_2$, respectively:

$$\boldsymbol{C}_{\tilde{i}_1}^{i_1} \approx \boldsymbol{I} + [\boldsymbol{\theta}_1\times], \tag{14}$$

$$\boldsymbol{C}_{\tilde{i}_2}^{i_2} \approx \boldsymbol{I} + [\boldsymbol{\theta}_2\times]. \tag{15}$$

At initial time t_0, $\boldsymbol{C}_{i_0}^{i_2}$ is same as $\boldsymbol{C}_{b_0}^{b_2}$. As a constant matrix, $\boldsymbol{C}_{i_0}^{i_2}$ shows the rotation matrix from i_0 to i_2 and still keep a fixed value, so $\boldsymbol{C}_{i_0}^{i_2} = \boldsymbol{C}_{b_0}^{b_2}$. So far, the hull deformation relationship between IMU1 and IMU2 with large misalignment angle and time delay is obtained:

$$\begin{aligned} &\{\boldsymbol{I} - [\boldsymbol{\theta}_2\times]\}\boldsymbol{C}_{b_0}^{b_2}\{\boldsymbol{I} - [\boldsymbol{\varphi}_0\times]\}\{\boldsymbol{I} + [\boldsymbol{\theta}_1\times]\}\cdot \\ &\boldsymbol{C}_{b_1}^{\tilde{i}_1}\{\boldsymbol{I} + [\boldsymbol{\varphi}_{10}\times]\}\boldsymbol{C}_{b_2}^{b_0} = \boldsymbol{C}_{b_2}^{\tilde{i}_2} + \dot{\boldsymbol{C}}_{b_2}^{\tilde{i}_2} \cdot \Delta\boldsymbol{t}. \end{aligned} \tag{16}$$

After multiplying by $\boldsymbol{C}_{b_0}^{b_2\mathrm{T}}$ on the left side and $\boldsymbol{C}_{b_1}^{\tilde{i}_1\mathrm{T}}$ on the right side, (13) can be derived as follows:

$$\begin{aligned} &\left\{\boldsymbol{I} - \left[\left(\boldsymbol{C}_{b_2}^{b_0}\boldsymbol{\theta}_2\right)\times\right]\right\}\{\boldsymbol{I} - [\boldsymbol{\varphi}_0\times]\}\{\boldsymbol{I} + [\boldsymbol{\theta}_1\times]\}\cdot \\ &\left\{\boldsymbol{I} + \left[\left(\boldsymbol{C}_{b_1}^{\tilde{i}_1}\boldsymbol{\varphi}_{10}\right)\times\right]\right\} = \boldsymbol{C}_{b_2}^{b_0}\left\{\boldsymbol{C}_{b_2}^{\tilde{i}_2} + \dot{\boldsymbol{C}}_{b_2}^{\tilde{i}_2} \cdot \Delta\boldsymbol{t}\right\}\boldsymbol{C}_{b_0}^{b_2}\boldsymbol{C}_{\tilde{i}_1}^{b_1}. \end{aligned} \tag{17}$$

Then (17) can be expressed as follows without consideration of high-order small quantity.

$$\begin{aligned} &\left\{\boldsymbol{I} + \left[\left(\boldsymbol{C}_{b_1}^{\tilde{i}_1}\boldsymbol{\varphi}_{10} + \boldsymbol{\theta}_1 - \boldsymbol{C}_{b_2}^{b_0}\boldsymbol{\theta}_2 - \boldsymbol{\varphi}_0\right)\times\right]\right\} = \\ &\boldsymbol{C}_{b_2}^{b_0}\left\{\boldsymbol{C}_{b_2}^{\tilde{i}_2} + \dot{\boldsymbol{C}}_{b_2}^{\tilde{i}_2} \cdot \Delta\boldsymbol{t}\right\}\boldsymbol{C}_{b_0}^{b_2}\boldsymbol{C}_{\tilde{i}_1}^{b_1}. \end{aligned} \tag{18}$$

Let $\boldsymbol{C}_{b_2}^{b_0}$, $\boldsymbol{C}_{b_2}^{\tilde{i}_2}$, and $\boldsymbol{C}_{b_1}^{\tilde{i}_1}$ be denoted by follows:

$$\begin{cases} \boldsymbol{C}_{b_2}^{b_0} = \begin{bmatrix} C_{11}^{20} & C_{12}^{20} & C_{13}^{20} \\ C_{21}^{20} & C_{22}^{20} & C_{23}^{20} \\ C_{31}^{20} & C_{32}^{20} & C_{33}^{20} \end{bmatrix} \\ \boldsymbol{C}_{b_2}^{\tilde{i}_2} = \begin{bmatrix} C_{11}^{2} & C_{12}^{2} & C_{13}^{2} \\ C_{21}^{2} & C_{22}^{2} & C_{23}^{2} \\ C_{31}^{2} & C_{32}^{2} & C_{33}^{2} \end{bmatrix} \\ \boldsymbol{C}_{b_1}^{\tilde{i}_1} = \begin{bmatrix} C_{11}^{1} & C_{12}^{1} & C_{13}^{1} \\ C_{21}^{1} & C_{22}^{1} & C_{23}^{1} \\ C_{31}^{1} & C_{32}^{1} & C_{33}^{1} \end{bmatrix} \end{cases}. \tag{19}$$

In order to simplify (18), $\boldsymbol{Z} = [Z(1), -Z(2), -Z(3)]^{\mathrm{T}}$ and $\boldsymbol{Z}_{\Delta t} = \mathrm{diag}([-Z_{\Delta t}(1), Z_{\Delta t}(2), Z_{\Delta t}(3)])$ are defined. And the elements in the vectors are shown as follows:

$$\begin{aligned} Z(1) = {} & C_{21}^{1}(C_{11}^{20}(C_{31}^{20}C_{11}^{2} + C_{32}^{20}C_{21}^{2} + C_{33}^{20}C_{31}^{2}) + \\ & C_{12}^{20}(C_{31}^{20}C_{12}^{2} + C_{32}^{20}C_{22}^{2} + C_{33}^{20}C_{32}^{2}) + C_{13}^{20}(C_{31}^{20}C_{13}^{2} + C_{32}^{20}C_{23}^{2} + \\ & C_{33}^{20}C_{33}^{2})) + C_{22}^{1}(C_{21}^{20}(C_{31}^{20}C_{11}^{2} + C_{32}^{20}C_{21}^{2} + C_{33}^{20}C_{31}^{2}) + \\ & C_{22}^{20}(C_{31}^{20}C_{12}^{2} + C_{32}^{20}C_{22}^{2} + C_{33}^{20}C_{32}^{2}) + C_{23}^{20}(C_{31}^{20}C_{13}^{2} + C_{32}^{20}C_{23}^{2} + \\ & C_{33}^{20}C_{33}^{2})) + C_{23}^{1}(C_{31}^{20}(C_{31}^{20}C_{11}^{2} + C_{32}^{20}C_{21}^{2} + C_{33}^{20}C_{31}^{2}) + \\ & C_{32}^{20}(C_{31}^{20}C_{12}^{2} + C_{32}^{20}C_{22}^{2} + C_{33}^{20}C_{32}^{2}) + \\ & C_{33}^{20}(C_{31}^{20}C_{13}^{2} + C_{32}^{20}C_{23}^{2} + C_{33}^{20}C_{33}^{2})) \end{aligned} \tag{20}$$

$$\begin{aligned} Z(2) = {} & C_{11}^{1}(C_{11}^{20}(C_{31}^{20}C_{11}^{2} + C_{32}^{20}C_{21}^{2} + C_{33}^{20}C_{31}^{2}) + C_{12}^{20}(C_{31}^{20}C_{12}^{2} + \\ & C_{32}^{20}C_{22}^{2} + C_{33}^{20}C_{32}^{2}) + C_{13}^{20}(C_{31}^{20}C_{13}^{2} + C_{32}^{20}C_{23}^{2} + C_{33}^{20}C_{33}^{2})) + \\ & C_{12}^{1}(C_{21}^{20}(C_{31}^{20}C_{11}^{2} + C_{32}^{20}C_{21}^{2} + C_{33}^{20}C_{31}^{2}) + C_{22}^{20}(C_{31}^{20}C_{12}^{2} + \\ & C_{32}^{20}C_{22}^{2} + C_{33}^{20}C_{32}^{2}) + C_{23}^{20}(C_{31}^{20}C_{13}^{2} + C_{32}^{20}C_{23}^{2} + C_{33}^{20}C_{33}^{2})) + \\ & C_{13}^{1}(C_{31}^{20}(C_{31}^{20}C_{11}^{2} + C_{32}^{20}C_{21}^{2} + C_{33}^{20}C_{31}^{2}) + C_{32}^{20}(C_{31}^{20}C_{12}^{2} + \\ & C_{32}^{20}C_{22}^{2} + C_{33}^{20}C_{32}^{2}) + C_{33}^{20}(C_{31}^{20}C_{13}^{2} + C_{32}^{20}C_{23}^{2} + C_{33}^{20}C_{33}^{2})) \end{aligned} \tag{21}$$

$$\begin{aligned} Z(3) = {} & C_{21}^{1}(C_{11}^{20}(C_{11}^{20}C_{11}^{2} + C_{12}^{20}C_{21}^{2} + C_{13}^{20}C_{31}^{2}) + C_{12}^{20}(C_{11}^{20}C_{12}^{2} + \\ & C_{12}^{20}C_{22}^{2} + C_{13}^{20}C_{32}^{2}) + C_{13}^{20}(C_{11}^{20}C_{13}^{2} + C_{12}^{20}C_{23}^{2} + C_{13}^{20}C_{33}^{2})) + \\ & C_{22}^{1}(C_{21}^{20}(C_{11}^{20}C_{11}^{2} + C_{12}^{20}C_{21}^{2} + C_{13}^{20}C_{31}^{2}) + C_{22}^{20}(C_{11}^{20}C_{12}^{2} + C_{12}^{20}C_{22}^{2} + \\ & C_{13}^{20}C_{32}^{2}) + C_{23}^{20}(C_{11}^{20}C_{13}^{2} + C_{12}^{20}C_{23}^{2} + C_{13}^{20}C_{33}^{2})) + \\ & C_{23}^{1}(C_{31}^{20}(C_{11}^{20}C_{11}^{2} + C_{12}^{20}C_{21}^{2} + C_{13}^{20}C_{31}^{2}) + C_{32}^{20}(C_{11}^{20}C_{12}^{2} + \\ & C_{12}^{20}C_{22}^{2} + C_{13}^{20}C_{32}^{2}) + C_{33}^{20}(C_{11}^{20}C_{13}^{2} + C_{12}^{20}C_{23}^{2} + C_{13}^{20}C_{33}^{2})) \end{aligned} \tag{22}$$

$$\begin{aligned} Z_{\Delta t}(1) = {} & C_{21}^{1}(C_{11}^{20}(C_{31}^{20}\dot{C}_{11}^{2}\mathrm{d}t + C_{32}^{20}\dot{C}_{21}^{2}\mathrm{d}t + C_{33}^{20}\dot{C}_{31}^{2}\mathrm{d}t) + \\ & C_{12}^{20}(C_{31}^{20}\dot{C}_{12}^{2}\mathrm{d}t + C_{32}^{20}\dot{C}_{22}^{2}\mathrm{d}t + C_{33}^{20}\dot{C}_{32}^{2}\mathrm{d}t) + C_{13}^{20}(C_{31}^{20}\dot{C}_{13}^{2}\mathrm{d}t + \\ & C_{32}^{20}\dot{C}_{23}^{2}\mathrm{d}t + C_{33}^{20}\dot{C}_{33}^{2}\mathrm{d}t)) + C_{22}^{1}(C_{21}^{20}(C_{31}^{20}\dot{C}_{11}^{2}\mathrm{d}t + C_{32}^{20}\dot{C}_{21}^{2}\mathrm{d}t + \\ & C_{33}^{20}\dot{C}_{31}^{2}\mathrm{d}t) + C_{22}^{20}(C_{31}^{20}\dot{C}_{12}^{2}\mathrm{d}t + C_{32}^{20}\dot{C}_{22}^{2}\mathrm{d}t + C_{33}^{20}\dot{C}_{32}^{2}\mathrm{d}t) + \\ & C_{23}^{20}(C_{31}^{20}\dot{C}_{13}^{2}\mathrm{d}t + C_{32}^{20}\dot{C}_{23}^{2}\mathrm{d}t + C_{33}^{20}\dot{C}_{33}^{2}\mathrm{d}t)) + C_{23}^{1}(C_{31}^{20}(C_{31}^{20}\dot{C}_{11}^{2}\mathrm{d}t + \\ & C_{32}^{20}\dot{C}_{21}^{2}\mathrm{d}t + C_{33}^{20}\dot{C}_{31}^{2}\mathrm{d}t) + C_{32}^{20}(C_{31}^{20}\dot{C}_{12}^{2}\mathrm{d}t + C_{32}^{20}\dot{C}_{22}^{2}\mathrm{d}t + \\ & C_{33}^{20}\dot{C}_{32}^{2}\mathrm{d}t) + C_{33}^{20}(C_{31}^{20}\dot{C}_{13}^{2}\mathrm{d}t + C_{32}^{20}\dot{C}_{23}^{2}\mathrm{d}t + C_{33}^{20}\dot{C}_{33}^{2}\mathrm{d}t)) \end{aligned} \tag{23}$$

$$\begin{aligned} Z_{\Delta t}(2) = {} & C_{11}^{1}(C_{11}^{20}(C_{31}^{20}\dot{C}_{11}^{2}\mathrm{d}t + C_{32}^{20}\dot{C}_{21}^{2}\mathrm{d}t + C_{33}^{20}\dot{C}_{31}^{2}\mathrm{d}t) + \\ & C_{12}^{20}(C_{31}^{20}\dot{C}_{12}^{2}\mathrm{d}t + C_{32}^{20}\dot{C}_{22}^{2}\mathrm{d}t + C_{33}^{20}\dot{C}_{32}^{2}\mathrm{d}t) + C_{13}^{20}(C_{31}^{20}\dot{C}_{13}^{2}\mathrm{d}t + \\ & C_{32}^{20}\dot{C}_{23}^{2}\mathrm{d}t + C_{33}^{20}\dot{C}_{33}^{2}\mathrm{d}t)) + C_{12}^{1}(C_{21}^{20}(C_{31}^{20}\dot{C}_{11}^{2}\mathrm{d}t + C_{32}^{20}\dot{C}_{21}^{2}\mathrm{d}t + \\ & C_{33}^{20}\dot{C}_{31}^{2}\mathrm{d}t) + C_{22}^{20}(C_{31}^{20}\dot{C}_{12}^{2}\mathrm{d}t + C_{32}^{20}\dot{C}_{22}^{2}\mathrm{d}t + C_{33}^{20}\dot{C}_{32}^{2}\mathrm{d}t) + \\ & C_{23}^{20}(C_{31}^{20}\dot{C}_{13}^{2}\mathrm{d}t + C_{32}^{20}\dot{C}_{23}^{2}\mathrm{d}t + C_{33}^{20}\dot{C}_{33}^{2}\mathrm{d}t)) + C_{13}^{1}(C_{31}^{20}(C_{31}^{20}\dot{C}_{11}^{2}\mathrm{d}t + \\ & C_{32}^{20}\dot{C}_{21}^{2}\mathrm{d}t + C_{33}^{20}\dot{C}_{31}^{2}\mathrm{d}t) + C_{32}^{20}(C_{31}^{20}\dot{C}_{12}^{2}\mathrm{d}t + C_{32}^{20}\dot{C}_{22}^{2}\mathrm{d}t + \\ & C_{33}^{20}\dot{C}_{32}^{2}\mathrm{d}t) + C_{33}^{20}(C_{31}^{20}\dot{C}_{13}^{2}\mathrm{d}t + C_{32}^{20}\dot{C}_{23}^{2}\mathrm{d}t + C_{33}^{20}\dot{C}_{33}^{2}\mathrm{d}t)) \end{aligned} \tag{24}$$

$$\begin{aligned} Z_{\Delta t}(3) = {} & C_{21}^{1}(C_{11}^{20}(C_{11}^{20}\dot{C}_{11}^{2}\mathrm{d}t + C_{12}^{20}\dot{C}_{21}^{2}\mathrm{d}t + C_{13}^{20}\dot{C}_{31}^{2}\mathrm{d}t) + \\ & C_{12}^{20}(C_{11}^{20}\dot{C}_{12}^{2}\mathrm{d}t + C_{12}^{20}\dot{C}_{22}^{2}\mathrm{d}t + C_{13}^{20}\dot{C}_{32}^{2}\mathrm{d}t) + C_{13}^{20}(C_{11}^{20}\dot{C}_{13}^{2}\mathrm{d}t + \\ & C_{12}^{20}\dot{C}_{23}^{2}\mathrm{d}t + C_{13}^{20}\dot{C}_{33}^{2}\mathrm{d}t)) + C_{22}^{1}(C_{21}^{20}(C_{11}^{20}\dot{C}_{11}^{2}\mathrm{d}t + C_{12}^{20}\dot{C}_{21}^{2}\mathrm{d}t + \\ & C_{13}^{20}\dot{C}_{31}^{2}\mathrm{d}t) + C_{22}^{20}(C_{11}^{20}\dot{C}_{12}^{2}\mathrm{d}t + C_{12}^{20}\dot{C}_{22}^{2}\mathrm{d}t + C_{13}^{20}\dot{C}_{32}^{2}\mathrm{d}t) + \\ & C_{23}^{20}(C_{11}^{20}\dot{C}_{13}^{2}\mathrm{d}t + C_{12}^{20}\dot{C}_{23}^{2}\mathrm{d}t + C_{13}^{20}\dot{C}_{33}^{2}\mathrm{d}t)) + C_{23}^{1}(C_{31}^{20}(C_{11}^{20}\dot{C}_{11}^{2}\mathrm{d}t + \\ & C_{12}^{20}\dot{C}_{21}^{2}\mathrm{d}t + C_{13}^{20}\dot{C}_{31}^{2}\mathrm{d}t) + C_{32}^{20}(C_{11}^{20}\dot{C}_{12}^{2}\mathrm{d}t + C_{12}^{20}\dot{C}_{22}^{2}\mathrm{d}t + \\ & C_{13}^{20}\dot{C}_{32}^{2}\mathrm{d}t) + C_{33}^{20}(C_{11}^{20}\dot{C}_{13}^{2}\mathrm{d}t + C_{12}^{20}\dot{C}_{23}^{2}\mathrm{d}t + C_{13}^{20}\dot{C}_{33}^{2}\mathrm{d}t)) \end{aligned} \tag{25}$$

From (16)−(25), the inertial measurement method equation of hull deformation with large misalignment angle and time delay can be described as follows after ignoring high-order small quantity:

$$\boldsymbol{Z} = \boldsymbol{C}_{b_1}^{\tilde{i}_1}\boldsymbol{\varphi}_{10} + \boldsymbol{\theta}_1 - \boldsymbol{C}_{b_2}^{b_0}\boldsymbol{\theta}_2 - \boldsymbol{\varphi}_0 + \boldsymbol{Z}_{\Delta t}\Delta\boldsymbol{t}. \tag{26}$$

3. System state equation and filter design for hull deformation

3.1 System state equation

According to (26), the state variables of system are established:

$$\boldsymbol{X} = [\boldsymbol{\varphi}_{10}\ \boldsymbol{\varphi}_0\ \boldsymbol{\theta}_1\ \boldsymbol{\theta}_2\ \boldsymbol{\varepsilon}_{1c}\ \boldsymbol{\varepsilon}_{2c}\ \boldsymbol{\varepsilon}_{1r}\ \boldsymbol{\varepsilon}_{2r}\ \Delta\boldsymbol{t}]. \tag{27}$$

The hull deformation angle $\boldsymbol{\varphi}_{10}$ consists of static deformation $\boldsymbol{\phi}_{\mathrm{st}}$ and dynamic deformation $\boldsymbol{\phi}_{\mathrm{dy}}$. The static deformation is described as a random walk process called quasi-static deformation because of its slow change [9]. The dynamic deformation is described as second-order Markov process [7]. $\boldsymbol{\varphi}_0$ is the initial angle between b_1 and b_0 at the initial time t_0.

$$\ddot{\boldsymbol{\phi}}_{\mathrm{st}} = \boldsymbol{w}_{\mathrm{st}} \tag{28}$$

$$\ddot{\boldsymbol{\phi}}_{\mathrm{dy}} = -2\mu\dot{\boldsymbol{\phi}}_{\mathrm{dy}} - b^2\boldsymbol{\phi}_{\mathrm{dy}} + 2b\sqrt{D\mu}\boldsymbol{w}_{\mathrm{dy}} \tag{29}$$

$$\dot{\boldsymbol{\varphi}}_0 = \boldsymbol{0} \tag{30}$$

where μ, λ, and D represent the irregular coefficient, main frequency, and variance of dynamic deformation angle, respectively. In addition, $b^2 = \mu^2 + \lambda^2$. $\boldsymbol{w}_{\mathrm{st}}$ and $\boldsymbol{w}_{\mathrm{dy}}$ represent the white noise of static deformation and dynamic deformation, respectively.

The gyro drift will cause the calculated coordinate sys-

tem to deviate from the ideal inertial coordinate system and form virtual drift angles of $\boldsymbol{\theta}_1$ and $\boldsymbol{\theta}_2$, respectively. After denoting $\boldsymbol{\varepsilon}_c$ as the gyro constant drift and $\boldsymbol{\varepsilon}_r$ as the gyro random drift, the drift angle [9] is described as follows:

$$\dot{\boldsymbol{\theta}}_1 = -\boldsymbol{C}_{b_1}^{i_1}(\boldsymbol{\varepsilon}_{1c} + \boldsymbol{\varepsilon}_{1r}), \tag{31}$$

$$\dot{\boldsymbol{\theta}}_2 = -\boldsymbol{C}_{b_2}^{i_2}(\boldsymbol{\varepsilon}_{2c} + \boldsymbol{\varepsilon}_{2r}). \tag{32}$$

The gyro constant drift $\boldsymbol{\varepsilon}_c$ is constant and the gyro random drift $\boldsymbol{\varepsilon}_r$ is modeled as first-order Markov model driven by white noise $\boldsymbol{w}_\varepsilon$:

$$\dot{\boldsymbol{\varepsilon}}_c = \boldsymbol{0}, \tag{33}$$

$$\dot{\boldsymbol{\varepsilon}}_r = -\mu_r \boldsymbol{\varepsilon}_r + \sigma\sqrt{2\mu_r}\boldsymbol{w}_\varepsilon. \tag{34}$$

$\Delta\boldsymbol{t} = [\ \Delta t_x, \Delta t_y, \Delta t_z]^{\mathrm{T}}$ represents the time delay between IMU1 and IMU2 and can be modeled as constant:

$$\Delta\dot{\boldsymbol{t}} = \boldsymbol{0}. \tag{35}$$

3.2 NNKF for spatio-temporal alignment

The two-layer parameters neural network is utilized to estimate the hull deformation angle. Neural network connection weights $\boldsymbol{W}$ is introduced into state variables of system of NNKF because of the tolerance of neural network in non-linearity [20]. Based on (27), the state variables of system are established as

$$\hat{\boldsymbol{X}} = [\boldsymbol{W} \quad \boldsymbol{\varphi}_0 \quad \boldsymbol{\theta}_1 \quad \boldsymbol{\theta}_2 \quad \boldsymbol{\varepsilon}_{1c} \quad \boldsymbol{\varepsilon}_{2c} \quad \boldsymbol{\varepsilon}_{1r} \quad \boldsymbol{\varepsilon}_{2r} \quad \Delta\boldsymbol{t}] \tag{36}$$

In (36), $\boldsymbol{W} = [\boldsymbol{W}_{\mathrm{In}} \quad b_{\mathrm{In}} \quad \boldsymbol{W}_{\mathrm{Out}} \quad b_{\mathrm{Out}}]$ is time-invariant. The number of neurons in the middle layer of the neural network is denoted as l. $\boldsymbol{W}_{\mathrm{In}}$ and $\boldsymbol{W}_{\mathrm{Out}}$ represent the input and the output coefficients, respectively:

$$\boldsymbol{W}_{\mathrm{In}} = \left[\left(\boldsymbol{W}_{\mathrm{In}}^1\right)^{\mathrm{T}}, \left(\boldsymbol{W}_{\mathrm{In}}^2\right)^{\mathrm{T}}, \left(\boldsymbol{W}_{\mathrm{In}}^3\right)^{\mathrm{T}}\right]^{\mathrm{T}}, \tag{37}$$

$$\boldsymbol{W}_{\mathrm{Out}} = \left[\left(\boldsymbol{W}_{\mathrm{Out}}^1\right)^{\mathrm{T}}, \left(\boldsymbol{W}_{\mathrm{Out}}^2\right)^{\mathrm{T}}, \cdots, \left(\boldsymbol{W}_{\mathrm{Out}}^l\right)^{\mathrm{T}}\right]^{\mathrm{T}}, \tag{38}$$

where $\boldsymbol{W}_{\mathrm{In}}^i = \left[W_{\mathrm{In}}^{i,1}, W_{\mathrm{In}}^{i,2}, \cdots, W_{\mathrm{In}}^{i,l}\right]^{\mathrm{T}}$ $(i = 1,2,3)$, and $\boldsymbol{W}_{\mathrm{Out}}^j = \left[W_{\mathrm{Out}}^{j,1}, W_{\mathrm{Out}}^{j,2}, W_{\mathrm{Out}}^{j,3}\right]^{\mathrm{T}}$ $(j = 1,2,\cdots,l)$.

$\boldsymbol{b}_{\mathrm{In}}$ and $\boldsymbol{b}_{\mathrm{Out}}$ represent the input and the output threshold values, respectively.

$$\boldsymbol{b}_{\mathrm{In}} = \left[b_{\mathrm{In}}^1, b_{\mathrm{In}}^2, \cdots, b_{\mathrm{In}}^l\right]^{\mathrm{T}} \tag{39}$$

$$\boldsymbol{b}_{\mathrm{Out}} = \left[b_{\mathrm{Out}}^1, b_{\mathrm{Out}}^2, b_{\mathrm{Out}}^3\right]^{\mathrm{T}} \tag{40}$$

By introducing the neural network into system filtering equation, the NNKF system filtering equation can be expressed as

$$\dot{\hat{\boldsymbol{X}}} = f\left(\hat{\boldsymbol{X}}\right) + \boldsymbol{w}, \tag{41}$$

$$\boldsymbol{Z} = \boldsymbol{C}_{b_1}^{\tilde{i}_1} g(\boldsymbol{Z}, \boldsymbol{W}) + H\left(\hat{\boldsymbol{X}}\right) + \boldsymbol{v}. \tag{42}$$

In system filtering equation, $\boldsymbol{w}$ and $\boldsymbol{v}$ are system state noise and measurement noise, respectively. $H(\hat{\boldsymbol{X}}) = \boldsymbol{\theta}_1 - \boldsymbol{C}_{b_2}^{b_0}\boldsymbol{\theta}_2 - \boldsymbol{\varphi}_0 + \boldsymbol{Z}_{\Delta t}\Delta\boldsymbol{t}$. The same $\boldsymbol{Z}$ as in (26) is the input of neural network , and the target output $g(\boldsymbol{Z}, \boldsymbol{W})$ is the $\boldsymbol{\varphi}_{10}$.

3.3 Process flow of spatio-temporal alignment method

Large misalignment angle and time delay often occur simultaneously. They will interact with each other and bring great challenges to the accuracy of hull deformation inertial measurement. To solve this problem, the spatio-temporal alignment method for hull deformation measurement is proposed.

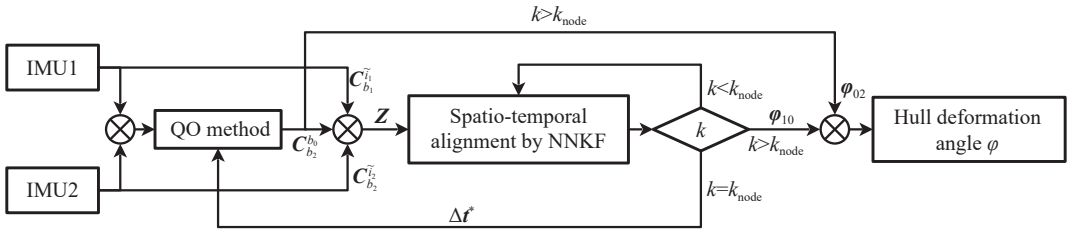

Fig. 4 Calculation flow chart of the proposed method

Fig. 4 shows the calculation flow chart of the spatio-temporal alignment method of hull deformation proposed in this paper. Two step loop design, i.e., time rough alignment and space rough alignment are designed to ensure the accurate measurement of hull deformation angle. In the first loop, due to the existence of time delay, the data dislocation effect leads to the relatively inaccurate coarse alignment results with large misalignment angle of the quaternion optimization (QO) method. Therefore, the spatio-temporal alignment method combined with NNKF is utilized to convert the problem into the rough estimation of the time delay under the condition of a certain misalignment angle, and the time delay rough alignment result $\Delta\boldsymbol{t}^*$ is obtained. The convergence point of the first

loop state is recorded as k_{node}. In the second loop, $\Delta \boldsymbol{t}^*$ is approximately converted into the number of sampling periods, and the sampling data of IMU1 and IMU2 are aligned together, so as to ensure the relative accuracy of the QO method result, thus guaranteeing the approximation of the small angle hypothesis of $\boldsymbol{\varphi}_{10}$. In this way, IMU1 attitude $\boldsymbol{C}_{b_1}^{\widetilde{i}_1}$, IMU2 attitude $\boldsymbol{C}_{b_2}^{\widetilde{i}_2}$ and large misalignment angle coarse alignment results $\boldsymbol{C}_{b_2}^{b_0}$ constitutes the observation variable together. Then the observation variable is substituted into the spatio-temporal alignment model, and NNKF is utilized to calculate $\boldsymbol{\varphi}_{10}$. Finally, inertial matching measurement results of hull deformation under the coexistence of time delay and large misalignment angle are obtained by adding the $\boldsymbol{\varphi}_{10}$ and $\boldsymbol{\varphi}_{02}$。

4. Experiments and analysis

In order to verify the effectiveness of the proposed method for hull measurement with large misalignment angle and time delay at the same time, the simulation experiment and turntable platform experiment are carried out.

4.1 Simulation experiment

The experiment is carried out at 118.097 7° east longitude and 24.439 0° north latitude. The accuracy of gyro in IMU is 0.008°/h, and the sampling frequency is 200 Hz. The static deformation angle is set as quasi-static deformation angle [9], which is simulated by sinusoidal signal with long period. The dynamic deformation angle is simulated as second-order Markov model, which is simulated by (29). The irregular coefficient is set as $\boldsymbol{\mu}_{\text{dy}} = [0.15, 0.10, 0.08]$; the main frequency is set as $\boldsymbol{\lambda}_{\text{dy}} = [0.24, 0.18, 0.11]$; the deformation variance is set as $\boldsymbol{D}_{\text{dy}} = \left[3.5\times10^{-7}, 1.8\times10^{-7}, 1.6\times10^{-7}\right]$. The hull angular motion $\boldsymbol{H}_i$ in three axial directions is simulated by sine signal as follows:

$$\boldsymbol{H}_i = \boldsymbol{\Phi}_i \sin(\boldsymbol{\omega}_i t + \boldsymbol{\varphi}_i) \tag{43}$$

where the hull motion swing amplitude is set as $\boldsymbol{\Phi}_i = [5°, 2°, 4°]^{\text{T}}$; the hull motion swing period is set as $\boldsymbol{T}_i = [8°, 6°, 10°]^{\text{T}}$; the hull motion initial phase is set as $\boldsymbol{\varphi}_i = [0°, 0°, 0°]^{\text{T}}$.

For convenience of expression, the time delay is abbreviated as TD, and the large misalignment angle is abbreviated as MA. In order to verify the performance of the proposed method in the face of misalignment angle and time delay, three methods are utilized for comparison. The three comparative methods are all inertial matching method for hull deformation, including the method without TD compensation and MA compensation (NoTD-NoMA), method only with TD compensation (TD-NoMA), method only with MA compensation (NoTD-MA). In order to control the variable, the time delay of NoTD-MA is set to a fixed value. The spatio-temporal alignment measurement method for hull deformation proposed in this paper is named as TD-MA.

The accuracy experiment is carried out with the 15 sampling periods of TD and the [6°, 3°, 2°] of MA between IMU1 and IMU2. Table 1 shows the compensation results of the TD and MA of the four comparison methods, and the corresponding result accuracy of root mean square error (RMSE). The NoTD-NoMA has the largest error in the four comparative methods. It is clear that the existence of TD and MA brings great challenges to the traditional hull deformation inertia matching method. TD-NoMA can effectively estimate TD and limit the estimation error of TD within one sampling period (5 ms). But restricted by the large misalignment angle, TD is not accurate enough. NoTD-MA has the ability to compensate for large misalignment angle under the condition of fixed time period. However, due to TD, the RMSE of NoTD-MA is still large, and the result error exist a big oscillation as shown in Fig. 5. It can be seen that MA mainly leads to the steady-state error of hull deformation estimation, and TD mainly leads to the drift and oscillation of hull deformation error, thus affecting the accurate measurement.

Table 1 Accuracy result of four comparative methods

Evaluating indicator	NoTD-NoMA	TD-NoMA	NoTD-MA	TD-MA
TD/ms	–	74.76	–	74.81
	–	73.85	–	74.87
	–	73.06	–	75.03
MA/arc min	–	–	407.99	359.05
	–	–	121.12	181.42
	–	–	257.91	120.16
RMSE/arc min	395.28	11.25	19.20	0.87
	199.44	5.75	118.21	0.29
	135.91	9.05	90.62	0.38

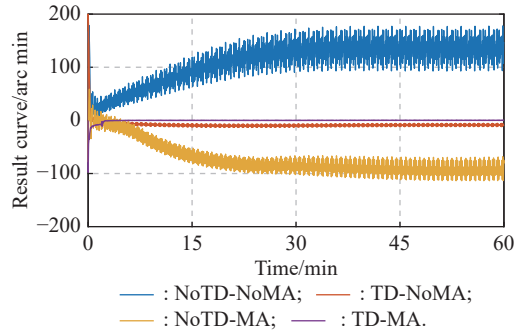

Fig. 5 Error curve of four comparative methods on *Z*-axis

TD-MA method, i.e., the spatio-temporal alignment method proposed in this paper can effectively compen-

sate TD and MA and get a smaller RMSE after the joint model calculation of TD and MA. Fig. 6 shows the estimation error curve of TD-MA method. Fig. 7 shows the estimation of TD by the proposed method, and Fig. 8 shows the estimation of MA by the proposed method. From the three figures, before the k_{node}, QO method cannot accurately estimate the MA due to the TD. After the $\Delta \boldsymbol{t}^*$ is estimated by the spatio-temporal alignment model and NNKF, the variable of state $\Delta \boldsymbol{t}^*$ is fed back to the QO method, the MA is calculated effectively. And the result of TD-MA can be accurately calculated by the new spatio-temporal alignment model to get a smaller RMSE, and the error oscillation of the result is relatively small.

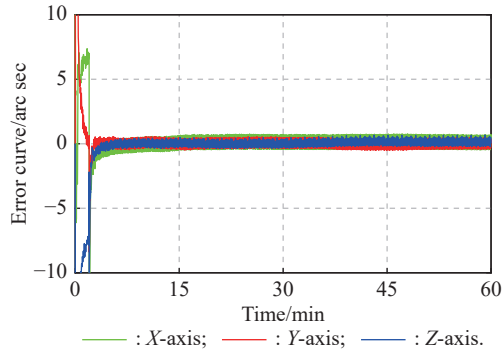

Fig. 6 Error curve of TD-MA method

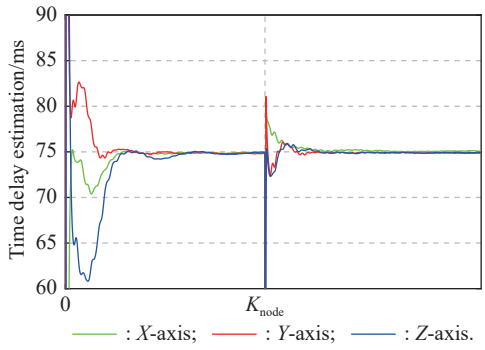

Fig. 7 Time delay estimation of TD-MA method

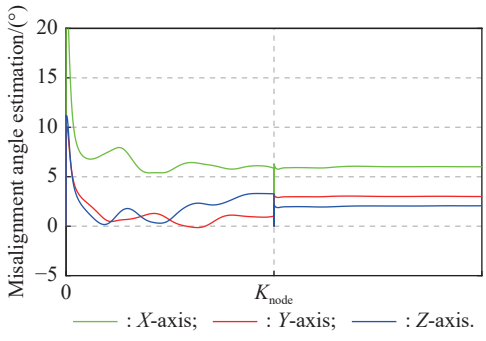

Fig. 8 Misalignment angle estimation of TD-MA method

In order to analyze the coexistence influence of TD and MA in the inertial matching measurement of hull deformation, the second part experiment is carried out ulteriorly. In this part of the experiment, the RMSE of four comparative methods are compared in Fig. 9−Fig. 11 under different combinations of TD and MA. The TD increases from 0 sampling period to 48 sampling period by six sampling period each time, where the sampling period is also 5 ms. The MA increases from 0° to 5° by 1° each time.

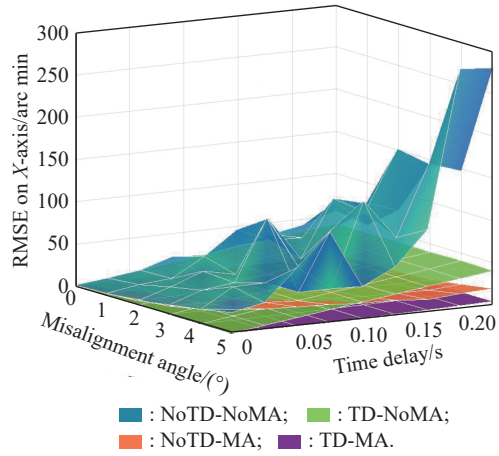

Fig. 9 Estimation result of the comparative methods under different time delays and misalignment angles on the *X*-axis

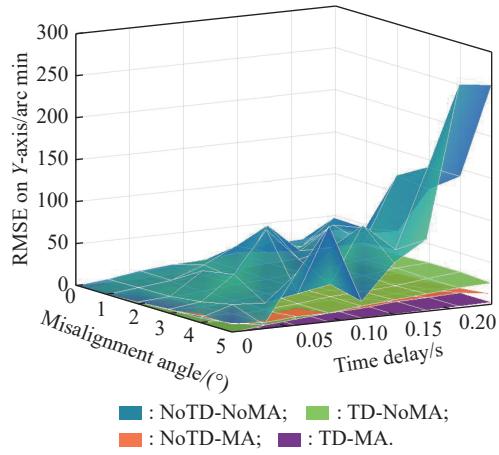

Fig. 10 Estimation result of the comparative methods under different time delays and misalignment angles on the *Y*-axis

In Fig. 9−Fig. 11, the RMSE of the NoTD-NoMA method shows a rapid growth with the increase of TD and MA, which indicates that the method faces great challenges under the interference of TD and MA coexistence. The TD-NoMA method has the ability of TD compensa-

tion. It can be seen from Fig. 9−Fig. 11 that the RMSE of the TD-NoMA method begins to increase with the increase of MA to a certain extent. Similarly, the MA compensation ability of the NoTD-MA method also reduces the error of this method, but with the increase of TD, the RMSE of the NoTD-MA method begins to increase greatly. When TD and MA coexist, the TD-NoMA method and the NoTD-MA method can restrain the error caused by the coexistence of TD and MA benefiting from one of the variable compensations in the model, but the existence of the other variable will still greatly affect the method accuracy.

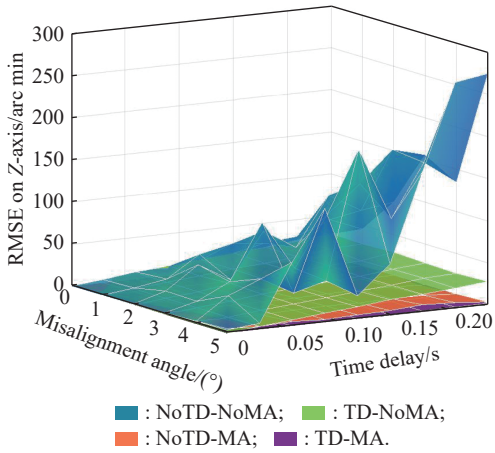

Fig. 11 Estimation result of the comparative methods under different time delays and misalignment angles on the *Z*-axis

The TD-MA method proposed in this paper is less affected by TD and MA and keeps a small RMSE, which verifies the effectiveness of the proposed algorithm for inertial matching measurement of hull deformation under the coexistence of time delay and large spatial misalignment angle.

4.2 Platform experiment

The platform experiment is carried out to verify the performance of the proposed method on the turntable.

The IMU is fixedly installed in the inner ring of the high-precision turntable, and synchronously connected with the upper computer through serial communication as shown in Fig. 12, whose output is excited by the three-axis sinusoidal motion of the turntable. The IMU accuracy is 0.008°/h, and the sampling period is 200 Hz.

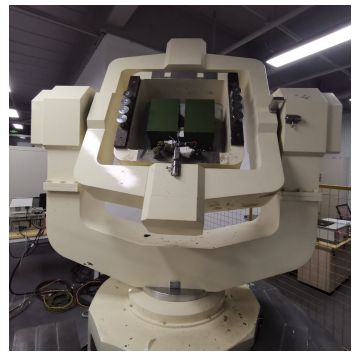

Fig. 12 Installation schematic diagram of IMU on the turntable

The hull deformation is simulated by quasi-static model and dynamic model, and the model parameters are the same as those in the simulation experiment. The hull deformation signal is added to IMU output signal through unified coordinate system transformation with large misalignment angle. The upper computer dislocates the IMU data to simulate the time delay sampling of hull deformation inertial measurement system. In the platform verification experiment, the time delay is set as 15 ms, and the misalignment angle is set as [6°,3°,2°], the estimation result of hull deformation angle in three axial directions are shown in Fig. 13−Fig. 15. Combined with the error curve of three axes estimation results as shown in Fig. 16, the performance analysis of the proposed method is as follows. In the previous estimation process, due to the influence of time delay on the coarse alignment results with large misalignment angle, the result error of the first loop is large, and only the trend of quasi-static deformation angle can be tracked. With the development of the second loop of the proposed spatio-temporal alignment method, the estimation results quickly converge to a smaller error range under the coexistence of large misalignment angle and time delay, which can accurately track quasi-static deformation and effectively suppress the oscillation effect of time delay on dynamic deformation in the inertial matching measurement, thus accurately describing the details of dynamic deformation angle.

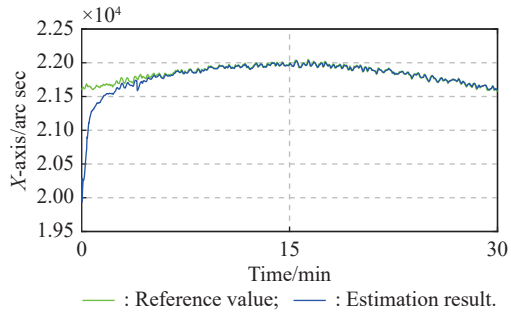

Fig. 13 Estimation result curve of hull deformation on *X*-axis

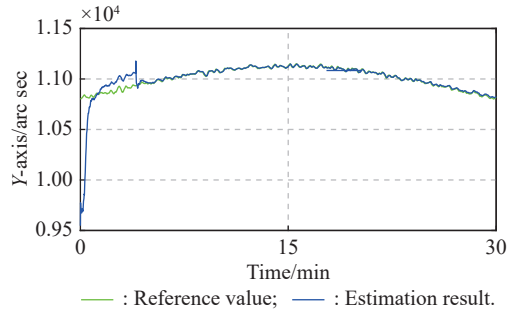

Fig. 14 Estimation result curve of hull deformation on *Y*-axis

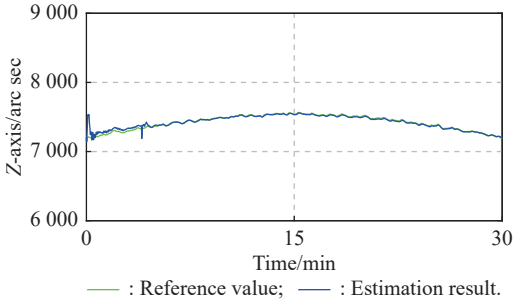

Fig. 15 Estimation result curve of hull deformation on *Z*-axis

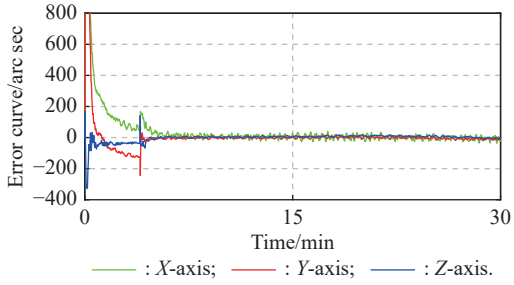

Fig. 16 Error curve in platform experiment

Fig. 17 and Fig. 18 show the time delay estimation result and the misalignment angle estimation result in the two step loops, respectively. In the first loop, the time delay is effectively converged by the proposed method, accompanied by inaccurate coarse alignment result of large misalignment, which leads to the low estimation accuracy of the proposed method in the early stage. In the second loop, the time delay converges more quickly and is brought into the model. Combined with the more accurate coarse alignment results of large misalignment angle after the time delay IMU data is aligned, so that the proposed algorithm can effectively track the quasi-static deformation angle and dynamic deformation angle under the coexistence of large misalignment angle and time delay, and the effectiveness of the proposed algorithm is verified.

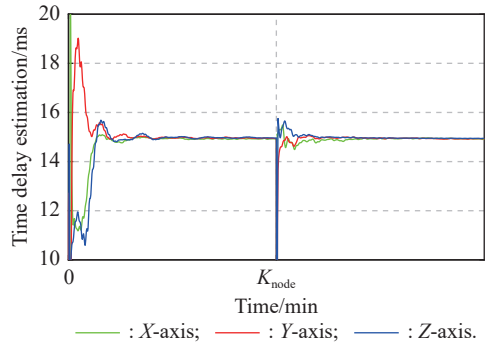

Fig. 17 Time delay estimation in platform experiment

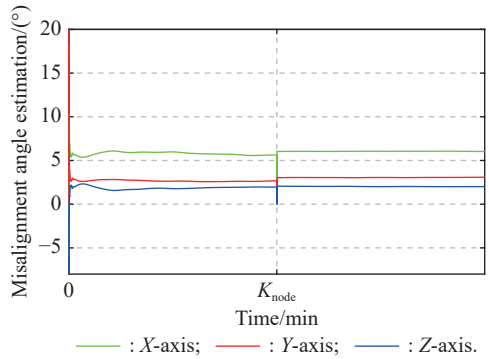

Fig. 18 Misalignment angle estimation in platform experiment

5. Conclusions

An improved spatio-temporal alignment inertial measurement method for hull deformation is proposed. The proposed method can complete the inertial measurement of hull deformation with a relatively small error under the joint influence of large misalignment angle and time delay. A brand-new hull deformation measurement model based on large misalignment angle coarse alignment and time delay modeling of IMU is derived. And the two steps control loop based on neural network Kalman filter is designed to ensure the synchronous alignment in space and time. The simulation experiments and turntable platform experiments illustrate the effectiveness of the proposed method.

References

[1] MENG Y, WANG W, HAN H, et al. A vision/radar/INS integrated guidance method for shipboard landing. IEEE Trans. on Industrial Electronics, 2019, 66(11): 8803–8810.

[2] WANG B, ZHU J W, MA Z X, et al. Improved particle filter-based matching method with gravity sample vector for underwater gravity-aided navigation. IEEE Trans. on Industrial Electronics, 2020, 68(6): 5206–5216.

[3] SHEN C, ZHANG Y, GUO X T, et al. Seamless GPS/inertial navigation system based on self-Learning square-root cubature Kalman filter. IEEE Trans. on Industrial Electronics, 2020, 68(1): 499–508.

[4] LI J C, GAO W, ZHANG Y, et al. Gradient descent opti-

mization-based self-alignment method for stationary SINS. IEEE Trans. on Instrumentation and Measurement, 2018, 68(9): 3278–3286.
[5] LIU H B, SUN C, ZHANG Y Q, et al. Hull deformation measurement for spacecraft TT&C ship by Photogrammetry. Science China Technological Sciences, 2015, 58: 1339–1347.
[6] GAO D, ZHENG J X, TAN W F, et al. Review on hull deformation measurement methods. Proc. of the AOPC 2020: Optical Sensing and Imaging Technology, 2020, 11567: 805−810.
[7] MOCHALOV A V, KAZANTSEV A V. Use of ring laser units for measurement of moving object deformations. Proc. of the 2nd International Conference on Lasers for Measurement and Information Transfer, 2002, 4680: 85–92.
[8] LEI S, XUE D X, SONG X G. Research on shafting alignment considering ship hull deformations. Marine Structures, 2010, 23(1): 103–114.
[9] ZHENG J X, QIN S Q, WANG X S, et al. Ship hull angular deformation measurement taking slow-varying quasi-static component into account. Journal of Chinese Inertial Technology, 2010, 19(1): 6–10.
[10] WEI W, SHENG C, QIN S Q. Online estimation of ship dynamic flexure model parameters for transfer alignment. IEEE Trans. on Control Systems Technology, 2013, 21(5): 1666–1678.
[11] WANG B, DENG Z Z, LIU C, et al. Estimation of information sharing error by dynamic deformation between inertial navigation systems. IEEE Trans. on Industrial Electronics, 2014, 61(4): 2015–2023.
[12] XU X, GUI J, SUN Y F, et al. A robust in-motion alignment method with inertial sensors and Doppler velocity log. IEEE Trans. on Instrumentation and Measurement, 2021, 70: 8500413.
[13] ZHOU Y M, WU W, QIN S Q. Approach for prediction of ship angular deformation based on distributed local inertial measurement units. Proc. of the 5th Symposium on Novel Optoelectronic Detection Technology and Application, 2019, 11023: 307−316.
[14] LI Y, WANG D, TONG J W. A hull deformation measurement method based on fiber optic gyro angular rate matching in complex sea conditions. Proc. of the Institution of Mechanical Engineers, Part M: Journal of Engineering for the Maritime Environment, 2022, 236(1): 34–47.
[15] ZHANG T, WANG J, JIN B N, et al. Application of improved fifth-degree cubature Kalman filter in the nonlinear initial alignment of strapdown inertial navigation system. Review of Scientific Instruments, 2019, 90(1): 015111.
[16] BING Z, MIAO W, XU J N, et al. Robust adaptive unscented Kalman filter and its application in initial alignment for body frame velocity aided strapdown inertial navigation system. Review of Scientific Instruments, 2018, 89(11): 115102.
[17] SHAO H J, MIAO L J, GAO W X, et al. Ensemble particle filter based on KLD and its application to initial alignment of SINS in large misalignment angles. IEEE Trans. on Industrial Electronics, 2018, 65(11): 8946–8955.
[18] XU B, DUAN T H, WANG Y F. An inertial measurement method of ship deformation based on IMM filtering. Optik, 2017, 140: 601–609.
[19] KRAMER K A, STUBBERUD S C, GEREMIA J A. Target registration correction using the neural extended Kalman filter. IEEE Trans. on Instrumentation and Measurement, 2010, 59(7): 1964–1971.
[20] HE Y, ZHANG X L, PENG X F, et al. Research on hull deformation measurement for large azimuth misalignment angle based on attitude quaternion. Optik, 2019, 182: 159–169.
[21] WANG Y Y, ZHANG Y, XU D J, et al. A deformation measurement algorithm based on adaptive variable parameter multiple model for large ships. IEEE Trans. on Instrumentation and Measurement, 2021, 70: 8504310.
[22] LU J Z, XIE L L, LI B G. Applied quaternion optimization method in transfer alignment for airborne AHRS under large misalignment angle. IEEE Trans. on Instrumentation and Measurement, 2016, 65(2): 346–354.

Biographies

XU Dongsheng was born in 1993. He received his B.S. degree from Northeastern University in 2016, and Ph.D. degree from Xiamen University in 2022. His current research interests include inertial measurement and multi-sensor fusion.
E-mail: xuds_xmu@163.com

YU Yuanjin was born in 1985. He received his B.S. degree from Huaqiao University in 2008, and Ph.D. degree from Beihang University in 2015. From 2015 to 2017, he was a post-doctoral fellow with Beihang University. From 2017 to 2018, he was a research assistant with University of Manchester. He is currently a professor with Beijing Institute of Technology. His research interests include control theory for engineering applications, and object detection and identification.
E-mail: yuanjin.yu@bit.edu.cn

ZHANG Xiaoli was born in 1970. He received his B.S. degree from Hebei University in 1992, M.S. degree from Northeast Normal University in 1995, and Ph.D. degree from Northeastern University in 2001. He is an associate professor with Xiamen University. His main research interests include inertial technology, and integrated navigation system.
E-mail: zhxl@xmu.edu.cn

PENG Xiafu was born in 1963. He received his B.S. degree from Harbin Engineering University in 1984, M.S. degree from Harbin Engineering University in 1994, and Ph.D. degree from Harbin Engineering University in 2001. He is a professor with Xiamen University. His research interests include intelligent unmanned vehicle system and inertial measurement.
E-mail: xfpeng@xmu.edu.cn